Human Molecular Genetics, 2014, Vol. 23, No. 11 **2914–2925**
doi:10.1093/hmg/ddu004
Advance Access published on January 12, 2014

FGFR3 mutation causes abnormal membranous ossification in achondroplasia

Federico Di Rocco[1,2,†], Martin Biosse Duplan[1,3,†], Yann Heuzé[4], Nabil Kaci[1], Davide Komla-Ebri[1], Arnold Munnich[1], Emilie Mugniery[1], Catherine Benoist-Lasselin[1] and Laurence Legeai-Mallet[1,*]

[1]INSERM U781, Université Paris Descartes, Sorbonne Paris Cité, Institut Imagine, Hopital Necker-Enfants malades, Paris, France [2]Neurochirurgie Pédiatrique Hôpital Necker Enfants malades, Unité de chirurgie craniofaciale, Paris, France [3]Service d'Odontologie, Hôpital Bretonneau, HUPNVS, AP-HP, Paris, France [4]Department of Anthropology, The Pennsylvania State University, University Park, PA, USA

Received November 1, 2013; Revised and Accepted January 2, 2014

***FGFR3* gain-of-function mutations lead to both chondrodysplasias and craniosynostoses. Achondroplasia (ACH), the most frequent dwarfism, is due to an *FGFR3*-activating mutation which results in impaired endochondral ossification. The effects of the mutation on membranous ossification are unknown. *Fgfr3*$^{Y367C/+}$ mice mimicking ACH and craniofacial analysis of patients with ACH and FGFR3-related craniosynostoses provide an opportunity to address this issue. Studying the calvaria and skull base, we observed abnormal cartilage and premature fusion of the synchondroses leading to modifications of foramen magnum shape and size in *Fgfr3*$^{Y367C/+}$ mice, ACH and FGFR3-related craniosynostoses patients. Partial premature fusion of the coronal sutures and non-ossified gaps in frontal bones were also present in *Fgfr3*$^{Y367C/+}$ mice and ACH patients. Our data provide strong support that not only endochondral ossification but also membranous ossification is severely affected in ACH. Demonstration of the impact of FGFR3 mutations on craniofacial development should initiate novel pharmacological and surgical therapeutic approaches.**

INTRODUCTION

Fibroblast growth factor receptors (FGFRs) are known to be important receptor tyrosine kinase (RTK) involved in skeletal development. *FGFR3* gain-of-function mutations lead to both chondrodysplasias and craniosynostoses. Among chondrodysplasias, achondroplasia (ACH), the most frequent genetic dwarfism is due to one recurrent transmembrane (TM) activating *FGFR3* mutation (p.Gly380Arg) that causes a structural change which affects both the stability and activity of FGFR3 dimers in the absence of ligand (1–4). Thanatophoric dysplasia (TD) type I and II are a lethal form in which a point mutation localized either in the extracellular (EC) or intracellular domain of *FGFR3* induces a dimerization of FGFR3 in the absence of ligand (5). Muenke syndrome (MS), the most common craniosynostosis syndrome, is also due to a single *FGFR3* gain-of-function mutation (p.Pro250Arg) in EC domain leading to varying effects on ligand-binding specificity (6–8). Finally, a rare form of craniosynostosis with skin disorder, a Crouzon syndrome with acanthosis nigricans (CAN), results from another TM *FGFR3* point mutation (p. Ala391Glu) localized in the same functional domain as ACH (9). The CAN TM mutation enhances the activity of the receptor in the absence of ligand and facilitates the activation of the tyrosine located in the activating loop (9,10). *FGFR3* mutations disturb several signaling pathways in chondrocytes and osteoblasts such as MAPK, P38, PLCγ, STAT and PKC pathways thus inducing anomalies of cellular proliferation, differentiation and/or apoptosis (11).

In order to understand the FGFR3-skeletal diseases, several mouse models have been generated, but they do not always faithfully and comprehensively mimic the human diseases. Mouse models of MS syndrome (*Fgfr3*^{P244R}) inconstantly share some phenotypic traits with the human disorder such as hearing loss and facial dysmorphology (12–14). Interestingly, the murine *Fgfr3*^{P244R} mutation does not only affect the skull but can also disturb the long bones (13). Numerous *Fgfr3*-related chondrodysplasia mouse models have been generated as well (15–17). Among them, we generated and studied the *Fgfr3*$^{Y367C/+}$ mice (18). These mutant mice present a severe dwarfism phenotype with a reduction of the length of the appendicular and axial

*To whom correspondence should be addressed. Email: laurence.legeai-mallet@inserm.fr
†These authors contributed equally to this work.

skeleton, consequence of a disturbed endochondral ossification (18–21). In these mice, we also noted that the overall shape of the skull was affected, with a domed cranial vault and an inverted bite (18,21). ACH patients present a similar craniofacial phenotype that is considered an endochondral ossification defect leading to shorter cranial base (22). The following issue therefore remains to be elucidated: is membranous ossification primarily affected in ACH? The availability of *Fgfr3*$^{Y367C/+}$ mice mimicking ACH provides an opportunity to address this issue by studying specifically the calvaria and skull base. In addition, the analysis of cranial anomalies in ACH and craniosynostosis syndromes (MS, CAN) offers the opportunity to compare the skull phenotype of three FGFR3-related diseases.

Here, we first provide evidence obtained through analysis of both *Fgfr3*$^{Y367C/+}$ mice and children with ACH showing that disruption of endochondral ossification result in skull base anomalies with premature fusion of the basal synchondroses and reduction of the size of the foramen magnum (FM). Then, studying the skull vault, we highlight a defective membranous ossification in *Fgfr3*$^{Y367C/+}$ mice and children with ACH. We observed non-ossified gap in frontal bones and a partial and premature fusion of sutures in both mice and children with ACH. Together, these data expand the general concept of dwarfism by showing that FGFR3 mutations affect not only the skull base and facial skeleton but also induce anomalies of the skull vault. This study sheds new light on the impact of *FGFR3* mutations on membranous ossification and could explain clinical hallmarks of ACH such as the macrocephaly and frontal bossing.

RESULTS

Fgfr3$^{Y367C/+}$ mice exhibit skull dysmorphy that mimics the human pathology

To evaluate the impact of the activating *Fgfr3* mutation (p.Tyr367Cys) on the craniofacial phenotype, we analyzed the growth of the skull of *Fgfr3*$^{Y367C/+}$ mice (21) and their control littermates at three different time-points: embryonic period (E16.5), birth (P0) and 3 weeks of age (P21). We focused on bones of the skull formed either by endochondral (nasal, occipital) or membranous (frontal, parietal, interparietal) ossification, whose developmental anomalies can contribute to overall skull dysmorphy. The macroscopic analysis of the cranium showed that a rounder shape of the head and shorter snout were present in *Fgfr3*$^{Y367C/+}$ mice at E16.5 compared with control littermates (Fig. 1A).

The severity of the dysmorphy worsened as the mice developed and increased from birth (Fig. 1B) to 3 weeks of age (Fig. 1C). This is similar to alterations of the long bones in *Fgfr3*$^{Y367C/+}$ mice that worsen in the first week of life (18). At 3 weeks of age, we observed a significant reduction in the length of the skull (66% of the control size, $P < 0.007$) (Fig. 1D).

The measurements of the size of each calvarial bone showed that the different bones are not equally affected by the *Fgfr3* mutation. We found a severe decrease in size in nasal (54% $P < 0.001$) and occipital bones (47%, $P < 0.001$), which are in accordance with anomalies in endochondral ossification (18). Focusing on bones formed by membranous ossification, the size of the interparietal bone was increased (125%, $P < 0.001$) (Fig. 1E), which could be a compensation of the reduced size of the occipital bone. No anomaly was observed in parietal bones, whereas the frontal bones were significantly reduced in size (82%, $P < 0.01$). We also observed the presence of a non-ossified gap in the frontal bones in all *Fgfr3*$^{Y367C/+}$ mice. The cellular origin of these bones formed by membranous ossification is different; the frontal bones are derived from cranial neural crest cells, whereas the parietal bones are derived from mesodermal cells (23). Interestingly, the mice expressing the *Fgfr3* mutation constitutively in mesoderm-derived tissues (Prx1,*Fgfr3*$^{Y367C/+}$) did not display frontal bone anomalies (data not shown). Our results show that the expression of *Fgfr3*$^{Y367C/+}$ mutation in neural crest-derived tissues causes an abnormal membranous ossification. Overall, the anomalies of the cranial bones in *Fgfr3*$^{Y367C/+}$ mice indicate that activated *Fgfr3* disrupted both endochondral and membranous ossification and allow to conclude that FGFR3 also contribute to the cranial vault development.

Next we compared the consequences on the craniofacial phenotype of *Fgfr3*-activating mutations in mice and humans. Viscerocranium and neurocranium were analyzed using μ-computed tomography (μCT) and CT scans. As observed on macroscopic preparations of the skulls, *Fgfr3*$^{Y367C/+}$ mice exhibited a domed macrocephalic cranium with an alteration of the frontal bones, a shorter snout and malocclusion at P21 (Fig. 2A). In humans, *FGFR3*-activating mutations induced various skeletal anomalies of the skull. Comparative analysis of CT scans of ACH, CAN (one child), MS patients and controls showed that the various *FGFR3* mutations do not alter the morphology of the skull in the same way, but all of them altered the growth of the skull vault (Fig. 2B). Interestingly, we observed consistently a large non-ossified gap in the skull vault of ACH and CAN patients (Fig. 2B). Though macrocephaly was present in the three conditions, the coronal sutures were usually fused in MS and CAN patients inducing a typical turribrachycephaly. In both conditions, the craniosynostosis might be severe and result in a cloverleaf shaped skull. Conversely, the alterations of the midface are absent in MS (24), whereas prognathism with reduced size of maxilla and mandible were found in ACH patients and in the CAN patient with cloverleaf skull studied here and others CAN patients reported previously (9,25,26). Many of these features are observed in mice carrying the mutation responsible for MS syndrome (*Fgfr3*^{P244R}) such as abnormal skull shape, reduced snout and malocclusion (12,27).

To further characterize these defects, we performed morphometric analyses in *Fgfr3*$^{Y367C/+}$ mice and children with ACH and their respective controls. We analyzed μCT and CT scan images of the skull using anatomical landmarks and geometric morphometrics (28). The principal components analysis (PCA) of the mouse skull shape separates the *Fgfr3*$^{Y367C/+}$ mice and their control littermates. When compared with their control littermates, the *Fgfr3*$^{Y367C/+}$ mice were characterized by a domed cranial vault, more vertical interparietal and occipital bones, an anteriorly and inferiorly projected FM, a shorter basioccipital bone, a shorter palate mainly because of an anteriorly reduced premaxilla, and a shorter snout (Fig. 2C). The modification of the posterior vault and position of the posterior sutures found in the *Fgfr3*$^{Y367C/+}$ mice could be explained by differences in growth of the occipital and interparietal bones (Figs 1E and 2C). Importantly, total or partial premature fusion of coronal,

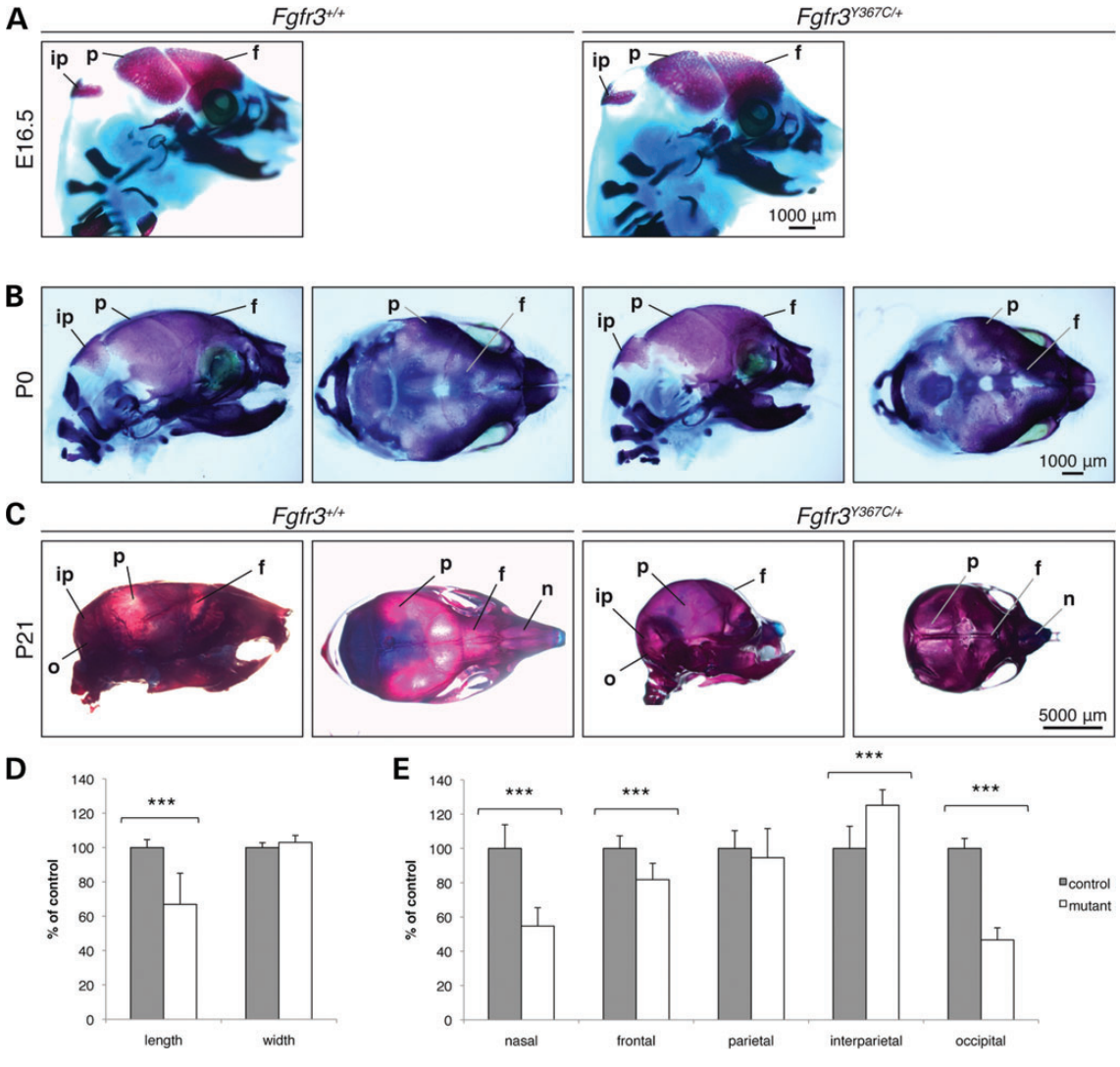

Figure 1. Macroscopic analysis of the skull of *Fgfr3*$^{Y367C/+}$ mice from antenatal to postnatal period. (**A**) Alizarin red and Alcian blue staining of the skull in *Fgfr3*$^{Y367C/+}$ ($n = 18$) compared with WT embryos ($n = 20$) at E16.5 of age showing the preliminary ongoing ossification. (**B**) Macroscopic analysis of the skull in *Fgfr3*$^{Y367C/+}$ ($n = 10$) compared with WT mice ($n = 11$) at birth (P0) showing a skull dysmorphy in mutant mice. (**C**) In P21 *Fgfr3*$^{Y367C/+}$ mice ($n = 41$) and WT mice ($n = 40$), a dramatic modification of the skull is present: the mutant mice display a turribrachycephaly with persistent defect of the medial skull vault at the level of frontal bone (non-ossified gap) with midface hypoplasia and inverted bite. (**D**) Measurements of the length and width of the skull of WT and *Fgfr3*$^{Y367C/+}$ mice at P21 showing a significant reduction of the length in mutant. (**E**) Measurements of the length of nasal, frontal, parietal, interparietal and occipital bones of *Fgfr3*$^{Y367C/+}$ mice versus WT, expressed as percentage of control. i.p. (interparietal), p (parietal), f (frontal) and o (occipital). $^{***}P < 0.001$.

frontonasal, squamous frontal and squamous parietal sutures were observed in all *Fgfr3*$^{Y367C/+}$ mice thus indicating that activated *Fgfr3* accelerated the closure of the sutures and disturbed osteogenesis in dwarf mice (Supplementary Material, Fig. S1).

In humans, the PCA of the human skull shape separated the ACH patients and the unaffected individuals. When compared with unaffected individuals, ACH patients were characterized by a domed cranial vault, an occipital bone more horizontally positioned but without a shorter posterior cranial fossa, a smaller FM, a shorter basioccipital bone, a shorter and flatter facial skeleton and a wider aspect of the most posterior facial skeleton (Fig. 2C). Focusing our analyses on sutures of the skull, we observed premature fusion of the sagittal and squamous sphenoidal sutures in ACH cases (3/6) (Supplementary Material, Fig. S1). This observation is consistent with recent papers reporting synostosis of multiple sutures in patients with ACH (29).

Our results revealed that the shape changes were highly similar in *Fgfr3*$^{Y367C/+}$ mice and ACH and that activated *FGFR3* disrupt membranous ossification in chondrodysplasia.

Fgfr3$^{Y367C/+}$ and human skull base anomalies appear during development

To evaluate the impact of activated *FGFR3* on the skull base, we focused our analyses on the spheno-occipital (SOS) and intra-occipital (IOS) synchondroses. At E16.5, macroscopic studies revealed no obvious abnormality (Fig. 3A). However, histological studies showed that in control mice, the cartilage

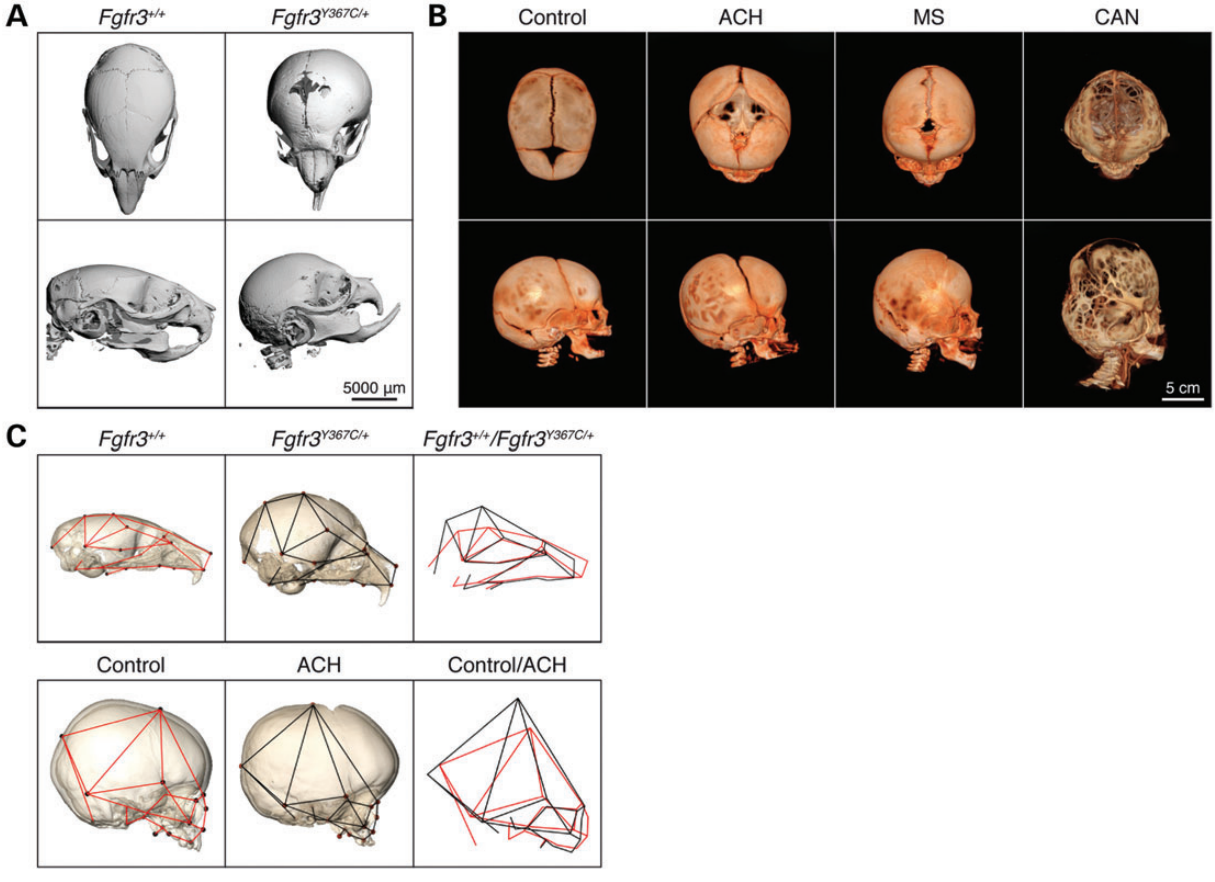

Figure 2. µCT of the head of *Fgfr3*$^{Y367C/+}$ mice and CT of ACH, MS, CAN patients with FGFR3-activating mutations. (**A**) µCT of *Fgfr3*$^{Y367C/+}$ ($n = 7$) and WT ($n = 7$) mice at P21 showing domed macrocephalic cranium with an impressive alteration of the vault and malocclusion in *Fgfr3*$^{Y367C/+}$ mice. (**B**) Representative CT of the skull at 3 months of age of control, ACH, MS and CAN patients. All FGFR3-related syndromes display macrocephaly and an altered shape of the skull. (**C**) Morphometric analyses of the *Fgfr3*$^{Y367C/+}$ mice ($n = 7$) versus their control littermates ($n = 7$), and ACH patients ($n = 6$) versus control patients of the same age ($n = 6$) showing the same modification of the skull vault and the midface. Superposition (Procrustes) of the consensus shape of the controls (red lines) and that of the mutants (black lines) showing similar anomalies.

was organized much like the growth plate cartilage of long bones, whereas in the *Fgfr3*$^{Y367C/+}$ mice, we observed a disorganized cartilage characterized by a smaller hypertrophic zone (Fig. 3B). At P0, the SOS anomaly was obvious with the sphenoid and occipital bones partially fused in most pups (6/7) (Fig. 3A). Both proliferative and hypertrophic zones were reduced, as was the size of the hypertrophic chondrocytes, revealed by Col X immunostaining (Fig. 3B). At P21, there was a total fusion of the SOS in all the mutants (Fig. 3A) and no hypertrophic chondrocytes were present (Fig. 3B). µCT scan analysis of the skull base confirmed this loss of SOS (Fig. 3C). Macroscopic and µCT analysis also showed that the IOS were fused in *Fgfr3*$^{Y367C/+}$ mice at P21 (Fig. 3C). The synchondroses defects are constant and severe compared with those reported in *Fgfr3*^{P244R} mice, where mild synchondroses anomalies are also present and lead to less premature closure of the IOS and SOS during development (12).

We next investigated the human cranial base in CT scans and observed a loss of SOS and IOS in ACH patients (Fig. 3D; Supplementary Material, Fig. S1) that was not found in MS or CAN (data not shown). The premature loss of the principal growth cartilage at the cranial base impaired postnatal growth of craniofacial bones and could explain some clinical hallmarks of ACH including hypoplasia of the midface and facial dysmorphy.

Fgfr3$^{Y367C/+}$ mice present an abnormal craniovertebral junction as in human pathology

To more firmly establish the extent of the anomalies at the craniovertebral junction in FGFR3-related disorders, we analyzed this region in both mouse model and human. µCT data of *Fgfr3*$^{Y367C/+}$ mice provided the opportunity to explore this area, in particular to look at the shape and size of the FM and atlas (C1). We observed a modification of FM in shape and size in *Fgfr3*$^{Y367C/+}$ mice at 3 weeks of age (Fig. 4A and B). The stenosis of the FM in *Fgfr3*$^{Y367C/+}$ mice affected the inner surface of the foramen with reduced sagittal (-20%; $P < 0.001$) and transverse (-40%; $P < 0.001$) diameters, modifying its shape. The inner transverse and sagittal diameters of the spinal canal at the level of C1 were also smaller in *Fgfr3*$^{Y367C/+}$ mice compared with controls (-25%; $P < 0.01$ and -10%; $P < 0.01$, respectively) (Fig. 4A and C). These alterations of craniovertebral junction are the consequence of both abnormal bone growth and premature fusion of cranial base synchondrosis.

In order to address the relevance to humans of these data, we measured in patients with FGFR3-related syndromes the size of the FM. It is established that the size of the FM in ACH patients is reduced (30). Here, we observed that the FM is not only reduced

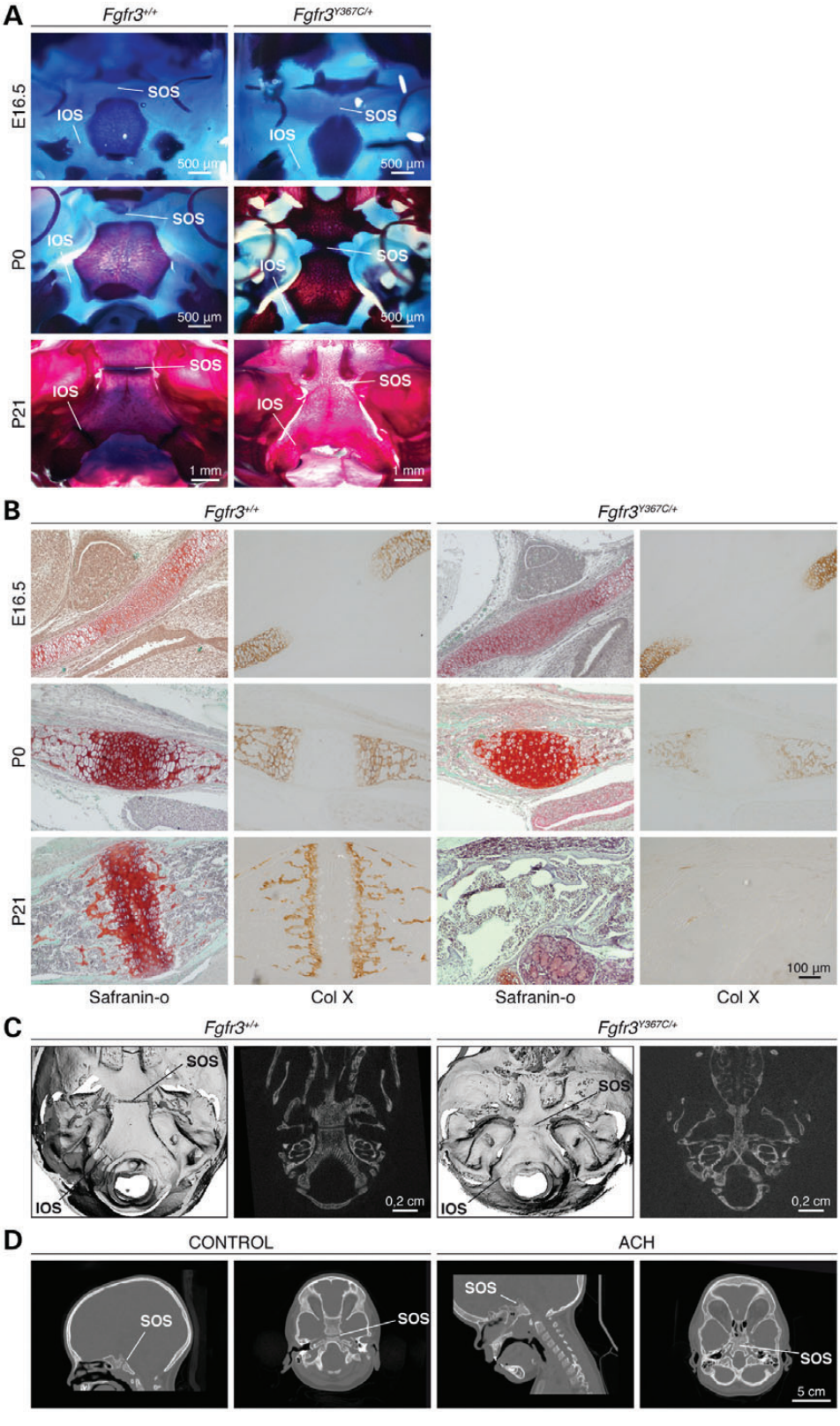

Figure 3. Analysis of the skull base of *Fgfr3*$^{Y367C/+}$ mice and ACH patients. (**A**) Macroscopic analysis of the skull base stained with Alizarin red and Alcian blue in control and mutant mice from E16.5 to 3 weeks of age (P21). Early fusion of the SOS and IOS during development in *Fgfr3*$^{Y367C/+}$ mice. (**B**) Histological analysis of SOS in E16.5 embryos, new born pups (P0) and 3-week-old mice (P21). The proliferative and hypertrophic zones of the cartilage are reduced in *Fgfr3*$^{Y367C/+}$ mice. An absence of SOS is observed at P21 in *Fgfr3*$^{Y367C/+}$ mice. (**C**) Representative µCT of WT ($n = 6$) and *Fgfr3*$^{Y367C/+}$ ($n = 6$) mice at P21 showing an absence of SOS and IOS in mutant. (**D**) Representative CT of ACH children (2 years old) and age-matched control showing the absence of SOS in ACH patient ($n = 6$) and its presence in controls ($n = 20$). SOS (spheno-occipital synchondrosis), IOS (intra-occipital synchondrosis).

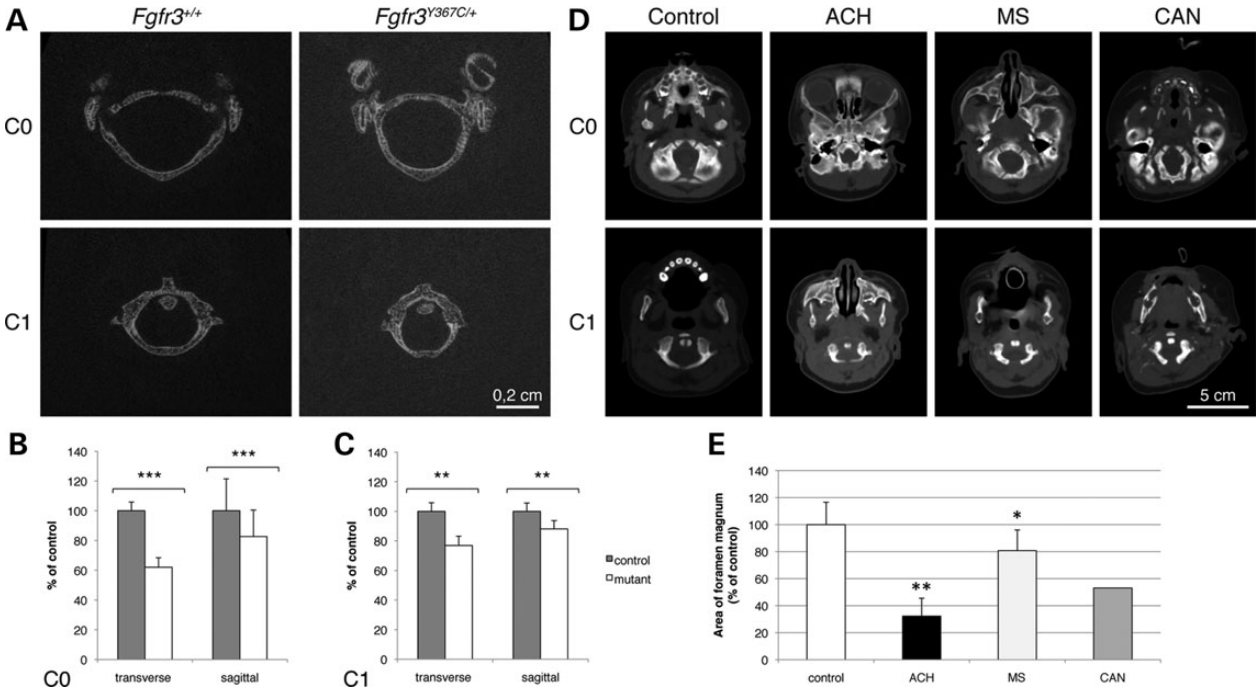

Figure 4. Reduction of the size of the FM in *Fgfr3*$^{Y367C/+}$ mice and ACH, MS, CAN patients with FGFR3-activating mutations. (**A**) Representative μCT of FM (C0) and atlas vertebra (C1) of *Fgfr3*$^{Y367C/+}$ mice and control littermate at 3 weeks of age. Modification of shape and size in mutant mice ($n = 7$). (**B**) Measurement of the transverse and sagittal length of C0 showing reduction of the size of C0 in *Fgfr3*$^{Y367C/+}$ mice ($n = 17$) compared with control ($n = 14$). (**C**) Measurement of the transverse and sagittal length of C1 showing reduction of the size of C1 in *Fgfr3*$^{Y367C/+}$ mice. (**D**) Representative CT of the FM at 3 months of age of control, ACH, MS and CAN patients. CT showing obvious reduction of the size of the FM in ACH and smaller reduction in MS and CAN. Measurement of the area of FM in control ($n = 20$, mean age 5.4 months), compared with ACH ($n = 6$, mean age 9.3 months), MS ($n = 8$, mean age 5.8 months) and CAN ($n = 1$, 3 months old) showing significant reduction of the size of ACH FM ($P < 0.001$) and MS ($P < 0.01$), $^{***}P < 0.001$, $^{**}P < 0.01$.

in ACH (32% of the size of controls; $P < 0.001$) but also in MS (81%; $P < 0.01$) and CAN patients (53%) (Fig. 4D and E). The degree of alteration of the FM is thus variable in FGFR3-related skeletal diseases and correlated to the severity of abnormal endochondral bone growth and the degree of fusion of the synchondroses.

Fgfr3$^{Y367C/+}$ mice exhibit cerebral alterations as in human pathology

To visualize the cervicomedullary junction at the level of the FM stenosis, we performed magnetic resonance imaging (MRI) of *Fgfr3*$^{Y367C/+}$ mice at 3 weeks of age. We observed severe brain alterations (Supplementary Material, Fig. S2A). The brain length was reduced by 20% ($P < 0.001$), and its height increased by 15% ($P < 0.01$) reflecting the skull modifications (Supplementary Material, Fig. S2B and C). When analyzing the posterior fossa, the neural structures in mutant mice appeared compressed and distorted when compared with controls. The cerebrospinal fluid (CSF) signal was reduced (Supplementary Material, Fig. S2D), especially at the level of the IV ventricle. No signs of hydrocephalus, ventricular dilation, nor increase of CSF subarachnoid spaces were found in mutant mice.

To address the relevance of these observations to human pathology, we used volumetric MRI analysis in humans identical to the methods used in *Fgfr3*$^{Y367C/+}$ mouse model. We found brain alterations in FGFR3-related diseases. In ACH, an enlargement of the subarachnoid spaces was commonly found (Supplementary Material, Fig. S2E) associated to a compression of the craniovertebral junction. These alterations were also present in another FGFR3-related chondrodysplasia, TD (data not shown) and in the CAN patient studied in this paper (Supplementary Material, Fig. S2E). In the great majority of MS patients, no compression of the craniovertebral junction and no hydrocephalus were found on MRI. Taken together, these results point toward the correlation between the size of FM and the significance of the cervicomedullary compression in FGFR3-related chondrodysplasia and craniosynostoses.

Fgfr3$^{Y367C/+}$ mice and human chondrodysplasia patients exhibit calvaria and coronal sutures defects

The skull vault consists mainly of flat bones formed by membranous ossification and separated by sutures. MS is characterized by uni or bilateral coronal suture synostosis (6,31). We tested here the hypothesis that activating Fgfr3 mutations disturb the suture development in dwarf mice and FGFR3-related chondrodysplasia. For that purpose, we analyzed coronal sutures of *Fgfr3*$^{Y367C/+}$ and control mice at E16.5, P0 and P21. We first confirmed that FGFR3 was present in the undifferentiated mesenchyme that separates the two fronts in *Fgfr3*$^{Y367C/+}$ coronal sutures at E16.5, P0 and P21 (data not shown) as in WT sutures (32). At P21, sagittal sections through the coronal sutures revealed that either (i) the two ossifications fronts, identified following Col I immunostaining, were fused or (ii) the overlap between the two

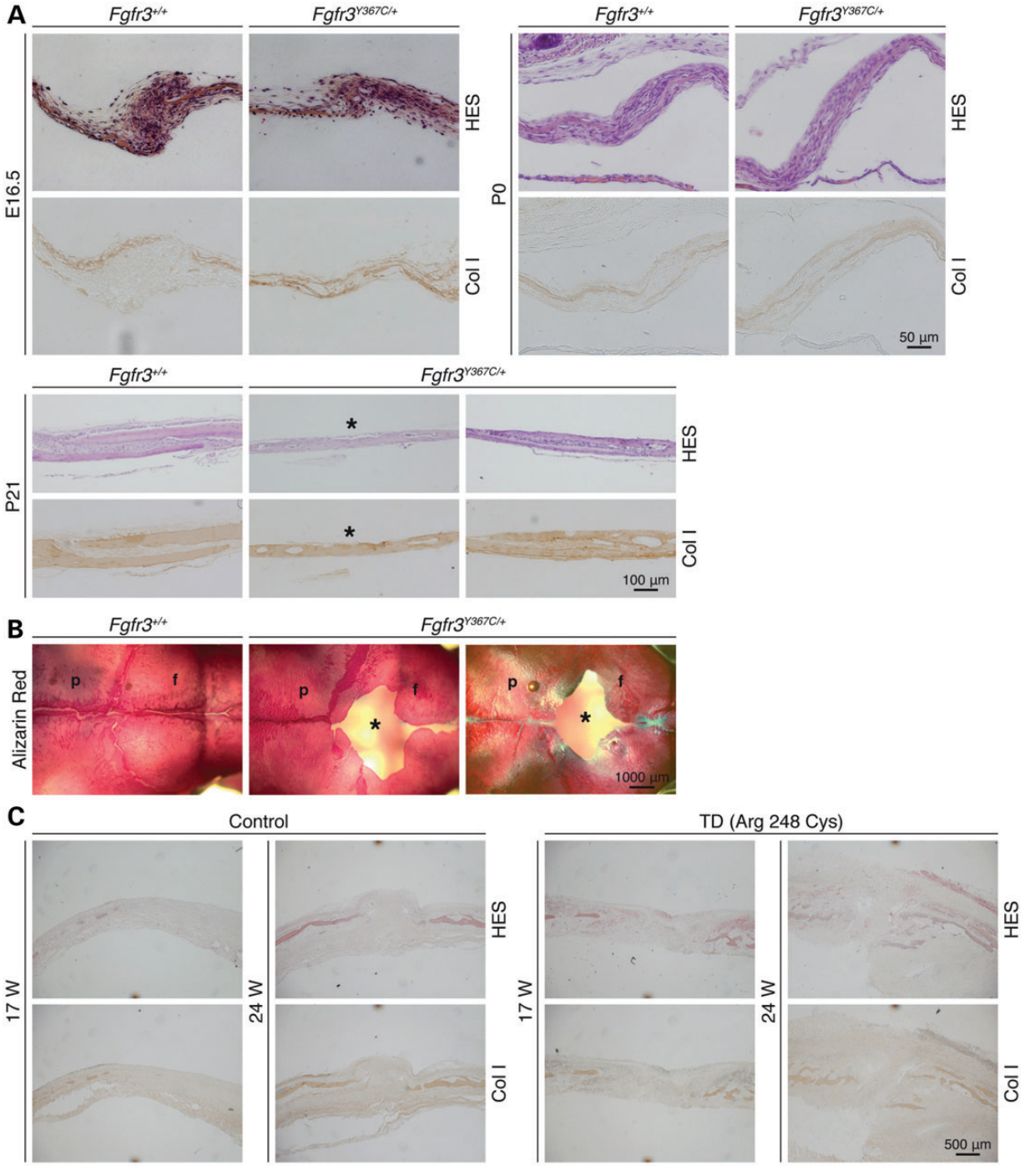

Figure 5. Partial fusion of the coronal suture in *Fgfr3*$^{Y367C/+}$ mice and TD patients. (**A**) Hematoxilin Eosin Safran (HES) staining of coronal sutures of E16.5, birth (P0), 3-week-old (P21) mutant and control mice. At P21, sutures are occasionally completely fused (*). Collagen type I (Col I) immunostaining of the coronal sutures, confirming the limits of the ossification fronts. (**B**) Macroscopic representation of the skull vault of *Fgfr3*$^{Y367C/+}$ mice and control littermates at 3 weeks of age stained with Alizarin red and Alcian blue. Impressive defect of the frontal bone (*) in mutant ($n = 13$) absent in control mice ($n = 14$). Sutures are occasionally completely fused and the overlap of the ossification fronts is increased. (**C**) Histological analysis of human coronal suture of TD ($n = 6$, aged 13–24 gestational weeks, mean age = 19.8) (TD) and age-matched control ($n = 6$, aged 16–26 gestational weeks, mean age = 21.5) fetuses. HES staining of coronal sutures and Col I immunostaining of the coronal sutures showing the premature fusion of TD suture compared with control at 17 and 24 gestational weeks. p (parietal), f (frontal).

fronts was increased (Fig. 5A). This is an important finding because in Muenke mouse model coronal suture fusion was a rare event (13).

Macroscopic examinations of P21 skull vaults confirmed the fusion or increased overlap of the ossifications fronts at the coronal suture, as well as an important medial non-ossified gap in *Fgfr3*$^{Y367C/+}$ affecting the two frontal bones anteriorly to the coronal suture (Fig. 5B). This defect was observed in >90% of the *Fgfr3*$^{Y367C/+}$ mice and was confirmed with µCT scans (Fig. 2A; Supplementary Material, Fig. S1).

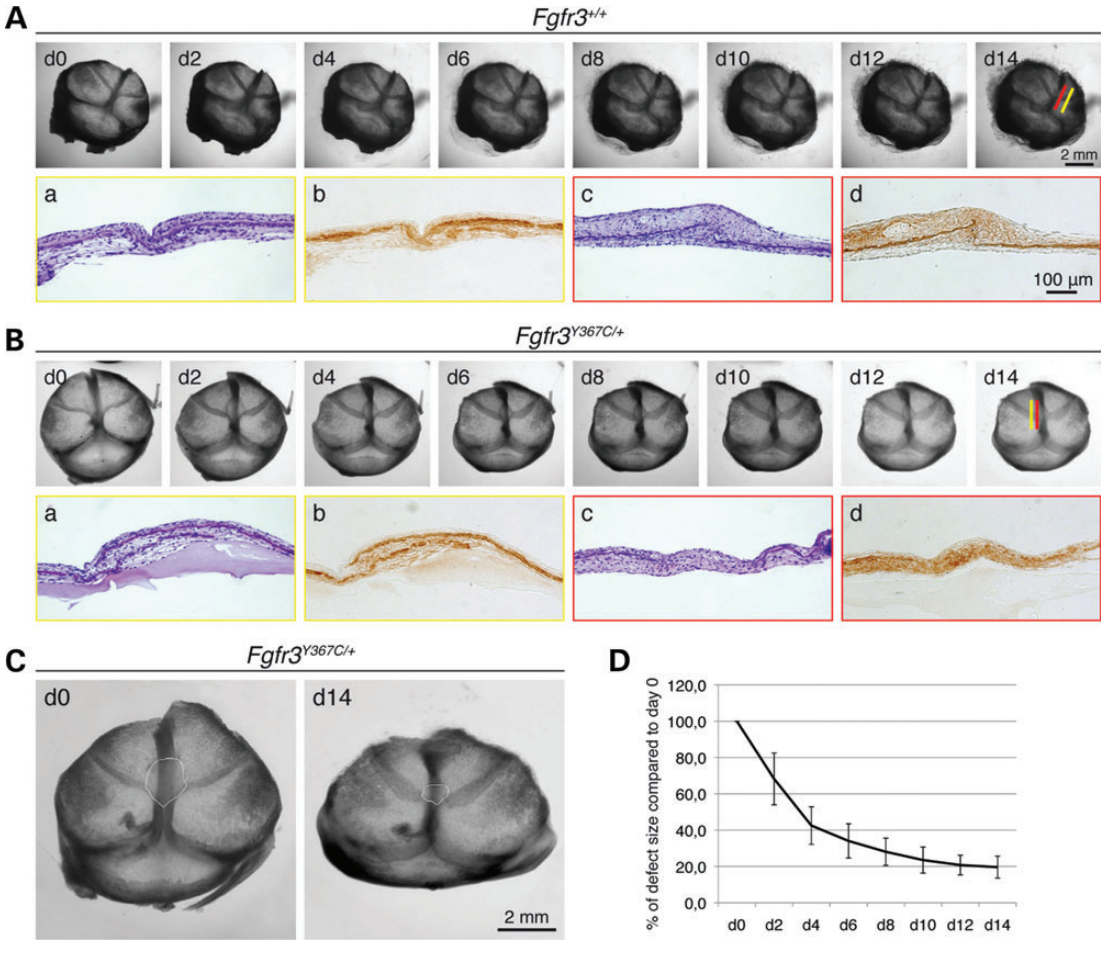

Figure 6. Culture of fetal calvaria isolated from *Fgfr3*$^{Y367C/+}$ mice and control littermate. (**A**) Representative images of the *ex vivo* culture of calvaria from control mice (*Fgfr3*$^{+/+}$) during 14 days ($n = 8$). HES staining and Col I immunostaining of the sutures revealed the absence of calvarial defect and limited overlap of ossifications fronts. Yellow line boxed images are representative images from sections of the coronal suture away from the sagittal midline, whereas red line boxed images are representative of sections closer to the midline. (**B**) Representative images of the *ex vivo* culture of calvaria from *Fgfr3*$^{Y367C/+}$ mice during 14 days ($n = 8$). HES staining and Col I immunostaining of the sutures revealed the presence of a large calvarial defect (red boxed) and increased overlap of ossifications fronts (yellow boxed). Yellow line boxed images are representative images from sections of the coronal suture away from the sagittal midline, whereas red line boxed images are representative of sections closer to the midline. (**C**) Higher magnification of the calvaria at Day 0 (d0) and Day 14 (d14) in *Fgfr3*$^{Y367C/+}$ mice. The calvarial defect is highlighted with a white line. (**D**) Evaluation of the reduction of the size of the calvaria defect during 14 days *ex vivo* culture in *Fgfr3*$^{Y367C/+}$ fetal mice ($n = 8$).

To parallel these analyses, we took opportunity of human coronal sutures isolated from TD, a severe and lethal form of chondrodysplasia associated with an *FGFR3*-activating mutation and age-matched control fetuses. At 17 weeks of gestational age, we observed an increased ossification of the coronal suture revealed by Col I immunostaining in TD when compared with age-matched controls (Fig. 5C). This premature fusion of the coronal suture in TD was even more pronounced at 24 weeks of age (Fig. 5C). These data, obtained in human coronal sutures, confirm the crucial role of FGFR3 in suture homeostasis during formation of the skull vault.

Fgfr3$^{Y367C/+}$ calvarial defects only partially resolve *ex vivo*

To add further support to the notion that *FGFR3* mutation disturbs skull vault, we next performed mouse calvarial *ex vivo* studies. Indeed, in ACH, it has been suggested that premature fusions of synchondrosis are responsible for the altered overall shape of the skull. It is therefore plausible that the observed defects of the cranial base may influence the fusion and growth of calvarial flat bones and contribute to the calvarial defect (foramina). In order to suppress any potential contribution of the cranial base to this defect, calvaria from *Fgfr3*$^{Y367C/+}$ and control embryos (E16.5) were dissected from the rest of the skull, separated from the influence of the brain and the cranial base and cultured *ex vivo* during 14 days (33). This strategy revealed that the cranial base and brain likely prevent the resolution of the defect since the size of the defect rapidly decreased when the calvaria was separated from the base (Fig. 6A and B). The defect regressed by >50% in 4 days (Fig. 6C and D). The defect however did not completely resolve and was still detected after 2 weeks of culture (Fig. 6B–D). Studying the coronal suture after 14 days of culture using Col I immunostaining, we observed anomalies characterized by an increase of the overlap between the two front of ossification (frontal and parietal bones). These data suggest that alterations of the underlying brain and skull base alone do not explain all the modifications we observed at the cranial vault and that activated *Fgfr3* induces an autonomous

membranous ossification delay of frontal bones. These results further confirm the role of FGFR3 in the vault formation and suture growth and fusion. Thus membranous ossification is disturbed by *FGFR3* mutations responsible for both chondrodysplasias and craniosynostoses.

DISCUSSION

This study arose from the observation that in humans, *FGFR3*-activating mutations result in ACH and MS where the bones predominantly affected are different: long bones formed by endochondral ossification in ACH and the parietal and frontal bones formed by membranous ossification in MS. It is usually considered that in ACH, endochondral ossification defects lead to reduced growth plate and fusion of synchondroses (22), while in MS membranous defects cause unilateral or bilateral premature fusion of coronal sutures (31). However, recent studies on patients and mouse models of FGFR3-related diseases, including this paper, draw a more complex picture. Here, we showed that in ACH patients and $Fgfr3^{Y367C/+}$ mice, the defective cranial phenotype is not the sole consequence of disturbed endochondral ossification but that membranous ossification is also affected.

In the developing skull base, we observed a severe defect of the endochondral ossification characterized by reduced size of the chondrocytes with a lack of organization, inducing synchondrosis premature fusion. This defect is similar to growth plate cartilage anomalies observed in $Fgfr3^{Y367C/+}$ mice, ACH and TD long bones (34) and confirms that activated FGFR3 disturbs all cartilages in the skeleton. Other reports on craniosynostosis and chondrodysplasia murine models support the evidence that FGFR3 and the Mapkinase pathway regulate synchondrosis closure (12,35,36). We also provided evidence that the synchondroses premature closure accounts for the FM stenosis and the cerebral alteration at posterior fossae in $Fgfr3^{Y367C/+}$ mice and ACH patients. These data correlate with clinical features of ACH (22,30). Interestingly, our study also demonstrated that in MS patients a significant reduction in the size of the FM was present suggesting that cranial base anomalies occur in craniosynostoses. The degree of reduction of FM area varied among FGFR3-related conditions with diverse clinical consequences; patients with ACH and CAN might need a surgical decompression of the craniovertebral junction, whereas in typical MS such surgical decompression is not needed. This spectrum of anomalies varying in FGFR3-related conditions may be due to the distinct impact of specific *FGFR3* mutations on chondrogenesis and osteogenesis during bone growth and highlight the complexity of RTK signaling in skeleton development. It was previously demonstrated that FGF signaling activates multiple downstream targets such as the mitogen-activated protein kinase pathway (21) and P38 (37) and synergizes with partners like transforming growth factor-β (38) and Wnt (39). The variable impact of FGFR3 mutations on endochondral ossification, limb and vertebral anomalies are reported not only in ACH but also in MS (40) and CAN syndromes (25). Interestingly, activating or loss-of-function mutations of FGFR1 and FGFR2, responsible for craniosynostosis, also induce defective long bone development (41).

The biological consequence of *FGFR3* mutations in craniosynostoses is a disruption of skeletal growth characterized by dysregulation of the intramembranous bone formation at the suture. The impairment of proliferation or accelerated differentiation of cranial osteoblasts leads to premature fusion of cranial sutures thus disturbing the expansion of the skull vault (42). Here, by investigating the skull vault of dwarf mice ($Fgfr3^{Y367C/+}$), we showed an alteration of membranous ossification with partial and premature fusion of the coronal sutures, and a reduced formation of the frontal bones, contrasting with the normal size of the parietal bones. To add further support to the notion that membranous ossification is affected in human pathology, we analyzed CT images of children with ACH and noted a delayed development of the frontal bones. Furthermore, we demonstrated that this ossification delay of the frontal bones was only partially rescued in calvaria cultured without skull base thus providing evidence that activated *FGFR3* affects specifically and autonomously membranous ossification. The high level of expression of *FGFR3* in the frontal bones compared with parietal bones (43) and this can also explain the difference in size (shorter frontals and normal parietals) due to the activating *FGFR3* mutation. We also analyzed ACH scans and TD coronal sutures by histology and we noted some degree of synostosis in coronal and sagittal sutures. Similar to our results, several cases of suture synostosis were reported in ACH patients (29,44,45), hypochondroplasia (MIM 146000) (46), mild dwarfism (47) and TD (48,49). Growth in the calvarial sutures is perpendicular to the orientation of the suture and is normally maintained throughout the period of growth of the brain. Synostosis of one or more sutures is accompanied by compensatory growth in other sutures and remodeling of other parts of the skull. Our data suggest thus that both synostosis and membranous ossification delay participate to the development of the prominent forehead observed in ACH. Here, we provide convincing data that abnormal FGF signaling leads to both synostoses and delay of membranous ossification.

This study highlights the impact of *FGFR3* mutations during cranial development in ACH and shows that both endochondral and intramembranous ossifications are primarily affected. The relevant hallmarks of ACH such as frontal bossing and macrocephaly might be the consequence of the disrupted membranous ossification. Demonstration of the impact of *FGFR3* mutations on craniofacial development should initiate novel pharmacological and surgical therapeutical approaches. $Fgfr3^{Y367C/+}$ mice will constitute a unique model to test these new strategies.

MATERIALS AND METHODS

Human subjects

All patients with craniosysnostoses and ACH were examined and followed at the Craniofacial Surgery Unit of Necker-Enfants Malades Hospital.

Children with MS ($n = 8$, mean age 5.8 months) and CAN ($n = 1$, 3 months old) presented with a brachycephaly due to a bicoronal synostosis and were operated on.

Coronal sutures were isolated from fetal skull derived from medically aborted control ($n = 6$) and TD ($n = 6$). Parents of all the subjects provided written, informed consent before recruitment into the study. Ethics approvals were obtained from the institutional review Board of Necker-Enfants Malades Hospital.

Mutational analysis of human FGFR3 gene

For the FGFR3 TM domain (ACH, CAN) and EC domain (MS), the primers used were described previously (2,6). Blood samples were obtained with the consents of the parents and were collected and processed in agreement with the French ethical committee guidelines.

Mouse models

WT and *Fgfr3*$^{Y367C/+}$ mice were generated by crossing *Fgfr3*^{neoY367C} mice (18) and Cmv-Cre mice (50). The mutant mice express the c.1100A > G (p.Tyr367Cys) mutation corresponding to the c.1118A > G (p.Tyr373Cys) in TD. All the mice were genotyped by PCR of tail DNA as described previously (18). All the experiments were conducted in *Fgfr3*$^{Y367C/+}$ mice, a mouse model that display parts of the clinical hallmarks of ACH (21). Experimental animal procedures and protocols were approved by the French Animal Care and Use Committee.

Whole-mount Alcian blue-Alizarin red staining

Calvariae of *Fgfr3*$^{Y367C/+}$ and their wild-type mice at E16.5, P0 and P21 were fixed in 95% ethanol and then stained with Alizarin red and Alcian blue, cleared by KOH treatment and stored in glycerol according to standard protocols (18). Size of the calvarial bones was measured on images captured with an Olympus PD70-IX2-UCB using cell sens software (Olympus).

Immunohistochemistry

Calvariae of *Fgfr3*$^{Y367C/+}$ and their wild-type littermates were fixed in 4% paraformaldehyde at 5°C, and decalcified in 0.5 M EDTA (pH 8.0) overnight or up to 1 week, depending on the age of the mice, and then dehydrated in graded series of ethanol, cleared in xylenes and embedded in paraffin. Five microns of sagittal sections were cut and stained with hematoxylin and eosin (H&E) and safrin-O and subjected to immunohistochemical staining using standard protocols using an antibody against FGFR3 (1:250 dilution; Sigma-Aldrich Co, St. Louis, MO, USA), anti-Col X (1:50 dilution; BIOCYC, Luckenwalde, Germany) and anti-Col I (1:500 for murine tissue, 1:1000 for human tissue, Novotec, Lyon, France) using the Dako Envision Kit (Dako North America, Inc, CA, USA). Same protocol was used for human coronal sutures. TD fetuses were obtained from legally terminated pregnancies according to the French ethical committee recommendations. The control group included spontaneously aborted fetuses showing no evidence of skeletal abnormalities. Images were captured with an Olympus PD70-IX2-UCB microscope (Olympus, Tokyo, Japan).

CT scanner of mouse and human

The head of the *Fgfr3*$^{Y367C/+}$ mice and their control littermates were imaged by μCT using a VivaCT40 microscanner (SCANCO Medical, Brüttisellen, Switzerland). All specimens from *Fgfr3*$^{+/+}$ and *Fgfr3*$^{Y367C/+}$ mice were scanned at the LBTO facility (INSERM U1059-IFR 143-IFRESIS St Etienne, France) using the following protocols (0.020 mm voxel resolution, 55 kV, Sigma 1.5/Support 2/Threshold 148, 150 μA).

Human scans were performed with a 64-slice CT system (LightSpeed VCT, General Electric Medical Systems, Milwaukee, WI, USA). The bone images were reconstructed in three dimensions using Carestream PACS v11.0 software (Carestream Health, Rochester, NY, USA).

Morphometric analysis

The samples consist of CT images of six patients diagnosed with ACH and six unaffected individuals matching on age the ACH patients (0.5–5 years), and of high-resolution CT images of seven P21 *Fgfr3*$^{Y367C/+}$ mice and seven control littermates. 3D coordinates of 31 landmarks were recorded on the reconstructed skulls of humans and mice and analyzed by geometric morphometric methods. Standardization for position, scale and orientation was obtained by Procrustes superimposition (51,52), and shape information (Procrustes coordinates) and size (centroid size; (52)) were extracted. Shape information was subsequently analyzed by PCA (for more information on geometric morphometrics applied to craniofacial birth defect, see, for example (28)). Wireframes are used to visualize the shape differences corresponding to the skull associated with specific scores on principal component 1 and 2.

Magnetic resonance imaging

All MRI were conducted on anesthetized (isoflurane) *Fgfr3*$^{+/+}$ and *Fgfr3*$^{Y367C/+}$ mice using a 4.7 T Bruker Biospec MR imager (Bruker BioSpin GmbH, Rheinstetten, Germany) at the Small Animal Imaging Facility of Paris Descartes University, INSERM, U970, Paris, France. The resolution was 0.0078 × 0.0078 cm/px × 625 μm/px for a matrix size of 256 × 256 × 32 with three averages and a repetition time of 1200 ms (echo time 80 ms) and two dummies scans. The total scan time was 30 min. Osirix software was used for postprocessing. For the quantification of CSF, after a midsagittal plane selection, a region of interest was drawn manually, delineating the posterior brain. The midsagittal slice (*S*) was normalized by subtracting *S* by Sm which was *S* filtered by a large median filter (5 × 5), resulting in a contrast image $C = S -$ Sm. The distribution of gray levels of *C* in brain tissue approximated a Gaussian behavior. Hence, bright CSF pixels corresponded to outliers for this Gaussian distribution. For CSF detection, we used one of the more current threshold (Th) used in 'box-and-whisker plots'. Th = Q75 + 1.5IQ, where Q75 and IQ are the 75 percentile and the interquartile range of *C* in the posterior brain, respectively. Then the fraction of pixels detected in the posterior brain (*FCSF*) was evaluated for each exam and *FCSF* values were compared between groups by a non-parametric Wilcoxon two-sample test. Difference between groups were considered significant for $P < 5\%$.

In human, MRI was performed with a 1.5T (Signa General Electric Medical Systems, Milwaukee, WI, USA) scanner using Carestream PACS v11.0 software (Carestream Health, Rochester, NY, USA). The MRI was performed without intravenous contrast enhancement.

Calvarial culture system

Ex vivo cultures were conducted as described previously (33) with slight modifications. E18.5 embryos were aseptically

dissected from the uterus of pregnant females and calvaria were separated from the rest of the skull after removal of the skin. The brain was detached form the calvaria and attention was paid not to remove the dura mater. Calvaria were then placed in 24-well plates, on top of 250 μl of Matrigel (BD Biosciences) previously placed at the bottom of the well. Calvaria were cultured in α-MEM (Gibco) supplemented with 10% fetal bovine serum (Gibco), 100 μg/ml ascorbic acid (Sigma) and 1% penicillin/streptomycin (Gibco). After 2 weeks, calvaria were separated from the gel, fixed in 4% paraformaldehyde at 4°C and embedded in paraffin. Serial sections of 5 mm were stained with H&E using standard protocols for histological analysis and submitted to immunohistological protocol. Images were captured with an Olympus PD70-IX2-UCB microscope. The size of the calvaria defect was measured using ImageJ software (NIH).

SUPPLEMENTARY MATERIAL

Supplementary Material is available at *HMG* online.

AUTHORS' CONTRIBUTIONS

F.D.R., M.B.D. and L.L.M. designed the mouse experiments, F.D.R. and A.M. implemented the clinical data, Y.H. generated CT data, M.D.B., N.K., D.K.E., E.M. and C.B.L. generated the data, F.D.R., M.B.D., Y.H. and L.L.M. analyzed the data; and F.D.R., M.B.D. and L.L.M. wrote the paper.

ACKNOWLEDGEMENTS

We thank Prof. Nathalie Boddaert for providing panel of control MRI (Hôpital Necker, Paris). We thank Dr Chiara Villa for her anatomopathological advices. We thank Gwennhael Autret and Daniel Balvay for MRI analyses (PIPA-ParisDescartes University) and Dr Laurence Vico and Norbert Laroche for μCT scanner analyses (LBTO INSERM U1059). We thank Dr Anne-Lise Delezoide, Dr B. Bessières and Dr J. Martinovic for providing the human suture samples. We thank Rachid Zoubairi for his work at the animal facility and Eric Le Gall for the artwork. We are grateful to the Association des Personnes de Petites Tailles and the Fondation des Gueules Cassées for supporting this work.

Conflicts of Interest statement. None declared.

WEB RESOURCE

www.omim.org.

REFERENCES

1. Naski, M.C., Wang, Q., Xu, J. and Ornitz, D.M. (1996) Graded activation of fibroblast growth factor receptor 3 by mutations causing achondroplasia and thanatophoric dysplasia. *Nat. Genet.*, **13**, 233–237.
2. Rousseau, F., Bonaventure, J., Legeai-Mallet, L., Pelet, A., Rozet, J.M., Maroteaux, P., Le Merrer, M. and Munnich, A. (1994) Mutations in the gene encoding fibroblast growth factor receptor-3 in achondroplasia. *Nature*, **371**, 252–254.
3. Shiang, R., Thompson, L.M., Zhu, Y.Z., Church, D.M., Fielder, T.J., Bocian, M., Winokur, S.T. and Wasmuth, J.J. (1994) Mutations in the transmembrane domain of FGFR3 cause the most common genetic form of dwarfism, achondroplasia. *Cell*, **78**, 335–342.
4. Placone, J. and Hristova, K. (2012) Direct assessment of the effect of the Gly380Arg achondroplasia mutation on FGFR3 dimerization using quantitative imaging FRET. *PLoS ONE*, **7**, e46678.
5. Rousseau, F., el Ghouzzi, V., Delezoide, A.L., Legeai-Mallet, L., Le Merrer, M., Munnich, A. and Bonaventure, J. (1996) Missense FGFR3 mutations create cysteine residues in thanatophoric dwarfism type I (TD1). *Hum. Mol. Genet.*, **5**, 509–512.
6. Muenke, M., Gripp, K.W., McDonald-McGinn, D.M., Gaudenz, K., Whitaker, L.A., Bartlett, S.P., Markowitz, R.I., Robin, N.H., Nwokoro, N., Mulvihill, J.J. *et al.* (1997) A unique point mutation in the fibroblast growth factor receptor 3 gene (FGFR3) defines a new craniosynostosis syndrome. *Am. J. Hum. Genet.*, **60**, 555–564.
7. Ibrahimi, O.A., Zhang, F., Eliseenkova, A.V., Linhardt, R.J. and Mohammadi, M. (2004) Proline to arginine mutations in FGF receptors 1 and 3 result in Pfeiffer and Muenke craniosynostosis syndromes through enhancement of FGF binding affinity. *Hum. Mol. Genet.*, **13**, 69–78.
8. Lajeunie, E., El Ghouzzi, V., Le Merrer, M., Munnich, A., Bonaventure, J. and Renier, D. (1999) Sex related expressivity of the phenotype in coronal craniosynostosis caused by the recurrent P250R FGFR3 mutation. *J. Med. Genet.*, **36**, 9–13.
9. Meyers, G.A., Orlow, S.J., Munro, I.R., Przylepa, K.A. and Jabs, E.W. (1995) Fibroblast growth factor receptor 3 (FGFR3) transmembrane mutation in Crouzon syndrome with acanthosis nigricans. *Nat. Genet.*, **11**, 462–464.
10. Chen, F., Sarabipour, S. and Hristova, K. (2013) Multiple consequences of a single amino acid pathogenic RTK mutation: the A391E mutation in FGFR3. *PLoS ONE*, **8**, e56521.
11. Marie, P.J., Miraoui, H. and Severe, N. (2012) FGF/FGFR signaling in bone formation: progress and perspectives. *Growth Factors (Chur, Switzerland)*, **30**, 117–123.
12. Laurita, J., Koyama, E., Chin, B., Taylor, J.A., Lakin, G.E., Hankenson, K.D., Bartlett, S.P. and Nah, H.D. (2011) The Muenke syndrome mutation (FgfR3(P244R)) causes cranial base shortening associated with growth plate dysfunction and premature perichondrial ossification in murine basicranial synchondroses. *Dev. Dyn.*, **240**, 2584–2596.
13. Twigg, S.R., Healy, C., Babbs, C., Sharpe, J.A., Wood, W.G., Sharpe, P.T., Morriss-Kay, G.M. and Wilkie, A.O. (2009) Skeletal analysis of the Fgfr3(P244R) mouse, a genetic model for the Muenke craniosynostosis syndrome. *Dev. Dyn.*, **238**, 331–342.
14. Mansour, S.L., Twigg, S.R., Freeland, R.M., Wall, S.A., Li, C. and Wilkie, A.O. (2009) Hearing loss in a mouse model of Muenke syndrome. *Hum. Mol. Genet.*, **18**, 43–50.
15. Naski, M.C., Colvin, J.S., Coffin, J.D. and Ornitz, D.M. (1998) Repression of hedgehog signaling and BMP4 expression in growth plate cartilage by fibroblast growth factor receptor 3. *Development*, **125**, 4977–4988.
16. Iwata, T., Chen, L., Li, C., Ovchinnikov, D.A., Behringer, R.R., Francomano, C.A. and Deng, C.X. (2000) A neonatal lethal mutation in FGFR3 uncouples proliferation and differentiation of growth plate chondrocytes in embryos. *Hum. Mol. Genet.*, **9**, 1603–1613.
17. Segev, O., Chumakov, I., Nevo, Z., Givol, D., Madar-Shapiro, L., Sheinin, Y., Weinreb, M. and Yayon, A. (2000) Restrained chondrocyte proliferation and maturation with abnormal growth plate vascularization and ossification in human FGFR-3(G380R) transgenic mice. *Hum. Mol. Genet.*, **9**, 249–258.
18. Pannier, S., Couloigner, V., Messaddeq, N., Elmaleh-Berges, M., Munnich, A., Romand, R. and Legeai-Mallet, L. (2009) Activating Fgfr3 Y367C mutation causes hearing loss and inner ear defect in a mouse model of chondrodysplasia. *Biochim. Biophys. Acta*, **1792**, 140–147.
19. Jonquoy, A., Mugniery, E., Benoist-Lasselin, C., Kaci, N., Le Corre, L., Barbault, F., Girard, A.L., Le Merrer, Y., Busca, P., Schibler, L. *et al.* (2012) A novel tyrosine kinase inhibitor restores chondrocyte differentiation and promotes bone growth in a gain of function Fgfr3 mouse model. *Hum. Mol. Genet.*, **21**, 841–851.
20. Mugniery, E., Dacquin, R., Marty, C., Benoist-Lasselin, C., de Vernejoul, M.C., Jurdic, P., Munnich, A., Geoffroy, V. and Legeai-Mallet, L. (2012) An activating Fgfr3 mutation affects trabecular bone formation via a paracrine mechanism during growth. *Hum. Mol. Genet.*, **21**, 2503–2513.
21. Lorget, F., Kaci, N., Peng, J., Benoist-Lasselin, C., Mugniery, E., Oppeneer, T., Wendt, D.J., Bell, S.M., Bullens, S., Bunting, S. *et al.* (2012) Evaluation of the therapeutic potential of a CNP analog in a Fgfr3 mouse model recapitulating achondroplasia. *Am. J. Hum. Genet.*, **91**, 1108–1114.
22. Horton, W.A., Hall, J.G. and Hecht, J.T. (2007) Achondroplasia. *Lancet*, **370**, 162–172.

23. Morriss-Kay, G.M. (2001) Derivation of the mammalian skull vault. *J. Anat.*, **199**, 143–151.
24. Ridgway, E.B., Wu, J.K., Sullivan, S.R., Vasudavan, S., Padwa, B.L., Rogers, G.F. and Mulliken, J.B. (2011) Craniofacial growth in patients with FGFR3Pro250Arg mutation after fronto-orbital advancement in infancy. *J. Craniofac. Surg.*, **22**, 455–461.
25. Arnaud-Lopez, L., Fragoso, R., Mantilla-Capacho, J. and Barros-Nunez, P. (2007) Crouzon with acanthosis nigricans. Further delineation of the syndrome. *Clin. Genet.*, **72**, 405–410.
26. Di Rocco, F., Collet, C., Legeai-Mallet, L., Arnaud, E., Le Merrer, M., Hadj-Rabia, S. and Renier, D. (2011) Crouzon syndrome with acanthosis nigricans: a case-based update. *Childs Nerv. Syst.*, **27**, 349–354.
27. Nah, H.D., Koyama, E., Agochukwu, N.B., Bartlett, S.P. and Muenke, M. (2012) Phenotype profile of a genetic mouse model for Muenke syndrome. *Childs Nerv. Syst.*, **28**, 1483–1493.
28. Heuze, Y., Boyadjiev, S.A., Marsh, J.L., Kane, A.A., Cherkez, E., Boggan, J.E. and Richtsmeier, J.T. (2010) New insights into the relationship between suture closure and craniofacial dysmorphology in sagittal nonsyndromic craniosynostosis. *J. Anat.*, **217**, 85–96.
29. Bessenyei, B., Nagy, A., Balogh, E., Novak, L., Bognar, L., Knegt, A.C. and Olah, E. (2013) Achondroplasia with multiple-suture craniosynostosis: a report of a new case of this rare association. *Am. J. Med. Genet. A*, **161**, 2641–2644.
30. Hecht, J.T., Horton, W.A., Reid, C.S., Pyeritz, R.E. and Chakraborty, R. (1989) Growth of the foramen magnum in achondroplasia. *Am. J. Med. Genet.*, **32**, 528–535.
31. Doherty, E.S., Lacbawan, F., Hadley, D.W., Brewer, C., Zalewski, C., Kim, H.J., Solomon, B., Rosenbaum, K., Domingo, D.L., Hart, T.C. *et al.* (2007) Muenke syndrome (FGFR3-related craniosynostosis): expansion of the phenotype and review of the literature. *Am. J. Med. Genet. A*, **143A**, 3204–3215.
32. Rice, D.P., Rice, R. and Thesleff, I. (2003) FGFR mRNA isoforms in craniofacial bone development. *Bone*, **33**, 14–27.
33. Perlyn, C.A., Morriss-Kay, G., Darvann, T., Tenenbaum, M. and Ornitz, D.M. (2006) A model for the pharmacological treatment of crouzon syndrome. *Neurosurgery*, **59**, 210–215; discussion 210–215.
34. Legeai-Mallet, L., Benoist-Lasselin, C., Munnich, A. and Bonaventure, J. (2004) Overexpression of FGFR3, Stat1, Stat5 and p21Cip1 correlates with phenotypic severity and defective chondrocyte differentiation in FGFR3-related chondrodysplasias. *Bone*, **34**, 26–36.
35. Sebastian, A., Matsushita, T., Kawanami, A., Mackem, S., Landreth, G.E. and Murakami, S. (2011) Genetic inactivation of ERK1 and ERK2 in chondrocytes promotes bone growth and enlarges the spinal canal. *J. Orthop. Res.*, **29**, 375–379.
36. Matsushita, T., Wilcox, W.R., Chan, Y.Y., Kawanami, A., Bukulmez, H., Balmes, G., Krejci, P., Mekikian, P.B., Otani, K., Yamaura, I. *et al.* (2009) FGFR3 promotes synchondrosis closure and fusion of ossification centers through the MAPK pathway. *Hum. Mol. Genet.*, **18**, 227–240.
37. Su, N., Sun, Q., Li, C., Lu, X., Qi, H., Chen, S., Yang, J., Du, X., Zhao, L., He, Q. *et al.* (2010) Gain-of-function mutation in FGFR3 in mice leads to decreased bone mass by affecting both osteoblastogenesis and osteoclastogenesis. *Hum. Mol. Genet.*, **19**, 1199–1210.
38. Chim, H., Manjila, S., Cohen, A.R. and Gosain, A.K. (2011) Molecular signaling in pathogenesis of craniosynostosis: the role of fibroblast growth factor and transforming growth factor-beta. *Neurosurg. Focus*, **31**, E7.
39. Krejci, P., Aklian, A., Kaucka, M., Sevcikova, E., Prochazkova, J., Masek, J.K., Mikolka, P., Pospisilova, T., Spoustova, T., Weis, M. *et al.* (2012) Receptor tyrosine kinases activate canonical WNT/beta-catenin signaling via MAP kinase/LRP6 pathway and direct beta-catenin phosphorylation. *PLoS ONE*, **7**, e35826.
40. Agochukwu, N.B., Solomon, B.D., Benson, L.J. and Muenke, M. (2013) Talocalcaneal coalition in Muenke syndrome: report of a patient, review of the literature in FGFR-related craniosynostoses, and consideration of mechanism. *Am. J. Med. Genet. A*, **161A**, 453–460.
41. Hatch, N.E. (2010) FGF signaling in craniofacial biological control and pathological craniofacial development. *Crit. Rev. Eukaryotic Gene Expression*, **20**, 295–311.
42. Wilkie, A.O. (1997) Craniosynostosis: genes and mechanisms. *Hum. Mol. Genet.*, **6**, 1647–1656.
43. Quarto, N., Behr, B., Li, S. and Longaker, M.T. (2009) Differential FGF ligands and FGF receptors expression pattern in frontal and parietal calvarial bones. *Cells Tissues Organs*, **190**, 158–169.
44. Georgoulis, G., Alexiou, G. and Prodromou, N. (2011) Achondroplasia with synostosis of multiple sutures. *Am. J. Med. Genet. A*, **155A**, 1969–1971.
45. Karadimas, C., Trouvas, D., Haritatos, G., Makatsoris, C., Dedoulis, E., Velissariou, V., Antoniadi, T., Hatzaki, A. and Petersen, M.B. (2006) Prenatal diagnosis of achondroplasia presenting with multiple-suture synostosis: a novel association. *Prenat. Diagn.*, **26**, 258–261.
46. Angle, B., Hersh, J.H. and Christensen, K.M. (1998) Molecularly proven hypochondroplasia with cloverleaf skull deformity: a novel association. *Clin. Genet.*, **54**, 417–420.
47. Bellus, G.A., McIntosh, I., Smith, E.A., Aylsworth, A.S., Kaitila, I., Horton, W.A., Greenhaw, G.A., Hecht, J.T. and Francomano, C.A. (1995) A recurrent mutation in the tyrosine kinase domain of fibroblast growth factor receptor 3 causes hypochondroplasia. *Nat. Genet.*, **10**, 357–359.
48. Tavormina, P.L., Shiang, R., Thompson, L.M., Zhu, Y.Z., Wilkin, D.J., Lachman, R.S., Wilcox, W.R., Rimoin, D.L., Cohn, D.H. and Wasmuth, J.J. (1995) Thanatophoric dysplasia (types I and II) caused by distinct mutations in fibroblast growth factor receptor 3. *Nat. Genet.*, **9**, 321–328.
49. Barroso, E., Perez-Carrizosa, V., Garcia-Recuero, I., Glucksman, M.J., Wilkie, A.O., Garcia-Minaur, S. and Heath, K.E. (2011) Mild isolated craniosynostosis due to a novel FGFR3 mutation, p.Ala334Thr. *Am. J. Med. Genet. A*, **155A**, 3050–3053.
50. Metzger, D., Clifford, J., Chiba, H. and Chambon, P. (1995) Conditional site-specific recombination in mammalian cells using a ligand-dependent chimeric Cre recombinase. *Proc. Natl. Acad. Sci. USA*, **92**, 6991–6995.
51. Rohlf, F.S.D. (1990) Extensions of the Procrustes method for the optimal superimposition of landmarks. *Syst. Zool.*, **39**, 40–59.
52. Dryden, I.L. and Mardia, K.V. (1998) *Statistical Shape Analysis*. Wiley, Chichester, UK.